Scattering of surface plasmon polaritons by impedance barriers: Dependence on angle of incidence

A. Yu. Nikitin,[1,3,*] G. Brucoli,[1] F. J. García-Vidal,[2] and L. Martín-Moreno[1,†]

[1]*Departamento de Física de la Materia Condensada-ICMA, Universidad de Zaragoza, E-50009 Zaragoza, Spain*
[2]*Departamento de Física Teórica de la Materia Condensada, Universidad Autónoma de Madrid, E-28049 Madrid, Spain*
[3]*Department of Theoretical Physics, A. Ya. Usikov Institute for Radiophysics and Electronics,*
Ukrainian Academy of Sciences, 12 Academician Proskura Strasse, 61085 Kharkov, Ukraine

This paper studies theoretically surface plasmon polariton scattering by one-dimensional defects of metal surface impedance at oblique incidence. Surface impedance boundary conditions are used to formulate an integral equation which can be solved both analytically and numerically to yield the transmission, reflection, and out-of-plane cross section as a function of angle of incidence and other parameters. Numerical calculations, as well as analytical expressions, obtained within the Born approximation are presented. Green's tensor approach is also applied so as to expand such analysis to region in which the surface impedance boundary conditions are not appropriate. We show that the angular dependencies for surface plasmon polariton scattering by impedance defects and by surface relief defects are essentially different. The angular dependency of surface plasmon polariton scattering by an impedance defect features an analog to Brewster's angle that is explained in terms of dipole polarization of the defect.

I. INTRODUCTION

Recent advances of nanotechnologies have disclosed a wide prospect for designing and realizing novel optical devices with applications in information processing and communication. Surface plasmon polariton (SPP) resonances could be employed to improve the efficiency of photonic circuits by increasing, for instance, the output power of surface emitting diodes[1] or decreasing the size of optical waveguides to a subwavelength scale.[2] When metallic elements are used, the high localization of electromagnetic field associated with SPPs can be exploited to guide light into volumes significantly smaller than the diffraction limit. However, the successful control of SPPs requires the implementation of optical elements for these surface modes such as mirrors, light emitters, multiplexers, and so forth.[3–5] It has been demonstrated, both theoretically and experimentally, that even shallow subwavelength surface defects or nanoparticles significantly scatter the incident energy from a SPP.[6–17] In particular, it has been shown that finite arrays of one-dimensional grooves or ridges behave as efficient Bragg's mirrors providing SPP band gaps in the appropriate frequency range.[9–12,15,16] It has also been shown that SPP scattering coefficients are very sensitive to the shape of a single scatterer.[8,15,16] Interestingly, the difference between the out-of-plane scattering cross sections for relief and impedance inhomogeneities is considerable, even when these inhomogeneities have the same spatial dependency.[15] The difference between the physical properties of SPPs produced at corrugated and impedance-modulated metal surfaces was also highlighted in Refs. 18 and 19. Remarkably, for each type of inhomogeneity, the width of the frequency band gap, $\Delta\omega$, arising from the coupling of SPPs, has a different dependence upon the angle ψ between the wave vectors. Namely, $\Delta\omega \sim |\cos\psi|$ for the periodical impedance modulation,[18,19] while $\Delta\omega \sim \sin(\psi/2)$ for the arrays of relief scatterers,[16] as

was also found experimentally (see Ref. 20). As a result, the SPP scattering coefficients should exhibit different angular dependencies for relief and impedance defects.

The aim of this paper is to examine the scattering of SPPs by one-dimensional (1D) defects of the surface impedance when the SPP angle of incidence is varied. Since it is much easier to measure the reflection coefficient at oblique incidence[10] than it is at normal incidence,[11] an investigation of the angle-dependent scattering amplitudes is relevant to possible experiments. We use two different theoretical methods: Green's tensor approach and Rayleigh expansion with surface impedance boundary conditions (SIBCs). Green's tensor approach (GTA) gives the exact result and provides analytical expressions for the long-distance behavior of scattered fields once the fields inside the defect are known. The solution based on the Rayleigh method and SIBCs allows for explicit analytical expressions of the scattering coefficients in the form of a Born series. As it will be shown, in some cases this helps with the physical interpretation of the scattering properties of the system. Both methods are compared so as to check the consistency and accuracy of the results obtained in the considered systems.

The paper is organized as follows: In Sec. II, we derive the pair of coupled integral equations for the Fourier amplitude of the scattered fields for both p and s polarizations. We discuss the difference between the scattering potential related to the impedance inhomogeneity and the one corresponding to relief defects. Section II C briefly highlights the application of GTA to the formulated problem. In Sec. III, we consider the scattering properties of a single defect illustrating the angular and shape dependencies. In the same section, we also compare the results computed using the Rayleigh expansion with the numerical results computed using GTA. Finally, Sec. IV deals with the Bragg SPP scattering by multiple impedance steps.

195441-1
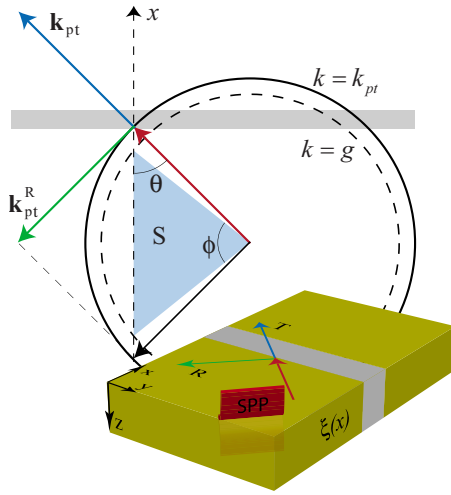
FIG. 1. (Color online) Schematic of the studied system: SPP scattering at the inhomogeneity formed by the perturbation of the surface impedance $\xi(x)$.

II. MODEL

A. Formulation of the problem

Consider a SPP with a unit electric field amplitude that propagates on a vacuum-metal interface and impinges at an angle θ onto a 1D perturbation of the surface impedance, $\xi(x)$. In terms of the dielectric permittivity of the metal, ϵ, the surface impedance is defined as $\xi = 1/\sqrt{\epsilon}$; see Fig. 1. In this paper, most of the results are obtained within the SIBCs, which are only valid for $|\epsilon| \gg 1$, so we will assume that $|\xi| \ll 1$. The incident SPP has harmonic time and spatial dependencies: $\exp(i\mathbf{k}_p \cdot \mathbf{r} - i\omega t)$, where $\mathbf{k}_p = g(q_p \cos \theta, q_p \sin \theta, \xi)$ is the SPP wave vector, $q_p = \sqrt{\epsilon/(1+\epsilon)} \simeq \sqrt{1-\xi^2}$, and $g = \omega/c = 2\pi/\lambda$. Let the z axis be directed into the metal. Absorption is expected to be negligible within the region of the defect provided the width of the impedance defect is much smaller than the SPP propagation length. Therefore, the metal is assumed to be lossless along the SPP path. We will enforce this simplification by using only the real part of the tabulated dielectric constants of the metals and setting $\text{Im}(\epsilon) = 0$. Nevertheless, in what follows, we will also show how absorption would affect the results. The diffraction problem is solved by the two independent methods highlighted below.

B. Rayleigh expansion

An impedance defect keeps the surface of a metal plane flat everywhere, so that the field can be represented exactly by a 1D integral expansion of the field over outgoing waves and waves decaying at $z \to -\infty$. This is in contrast to the case of relief inhomogeneities, wherein the Rayleigh expansion is valid only for shallow perturbations of the profile.[8,14–16]

If we omit the harmonic time dependency of the field, we can write the total electric field in the vacuum half-space as

$$\mathbf{E}(\mathbf{r}) = \mathbf{e}_p \exp(i\mathbf{k}_p \cdot \mathbf{r}) + \int dk \mathbf{E}_k \exp(i\mathbf{K} \cdot \mathbf{r}), \qquad (1)$$

where the wave vectors of scattered plane waves, $\mathbf{K} = (k, gq_p \sin \theta, k_z)$, have z components,

$k_z = \sqrt{g^2 - (gq_p \sin \theta)^2 - k^2}$, satisfying the radiation condition $\text{Im}(k_z) \geq 0$. The unit vector pointing along the electric field of an incoming SPP is $\mathbf{e}_p = (\xi \cos \theta, \xi \sin \theta, -q_p)$.

Assuming the metal to be highly reflective, $|\xi| \ll 1$, we use the well-known SIBCs, thus reducing the problem to finding the field in the vacuum half-space only. After some algebra (which is explained in Appendix A), we arrive at a pair of coupled integral equations for the two polarization components of the normalized Fourier field harmonics equation (A4). The solution of the integral equations yields the electromagnetic field at any point of the vacuum half-space. However, only the asymptotic expressions of the fields are needed for the calculation of the transmission T, reflection R, and out-of-plane scattering coefficient S.

C. Green's tensor approach

GTA is a very general treatment for tackling the scattering of light by inhomogeneities within a stratified medium. The theory in its generality has already been illustrated elsewhere.[21–26] Here, we provide a brief summary and some considerations on the technique relevant to the calculations carried out for an impedance defect. In Appendixes B and C, we will also focus on the semianalytical expansions of GTA which allow for the calculation of T, R, and S for such system.

Although the considered impedance defect is infinite along both the y and the z axes, it can be represented by a two-dimensional inhomogeneity of the metal dielectric permittivity with a finite depth in coordinate z as long as this depth is much greater than the skin depth of both the background metal and the defect. For example, we find that the scattering coefficients of an aluminum defect with a depth of 30 nm in the silver half-space differs only by 2% with respect to the infinite depth case (for a defect width of 200 nm and $\lambda = 600$ nm). Such depth is ≈ 2 skin depths in aluminum. In all GTA calculations shown, a defect of depth of 40 nm was used to simulate a defect of infinite depth.

The electric field is computed by solving the Lippmann–Schwinger equation,

$$\mathbf{E}(\mathbf{r}_\parallel) = \mathbf{E}_0(\mathbf{r}_\parallel) + g^2 \int_A (\epsilon_i - \epsilon)\hat{G}(\mathbf{r}_\parallel, \mathbf{r}'_\parallel)\mathbf{E}(\mathbf{r}'_\parallel)d\mathbf{r}'_\parallel, \qquad (2)$$

where $\mathbf{r}_\parallel = (x, 0, z)$, the integration region A is the inhomogeneity area, and ϵ_i and ϵ are the dielectric permittivities of the defect and the background metal, respectively. $\mathbf{E}_0$ is the incident field of a SPP. We will omit the y dependency of the field since it is cyclic with a constant spatial period k_{py}. $\hat{G}(\mathbf{r}_\parallel, \mathbf{r}'_\parallel)$ is Green's tensor (GT) for the vacuum-background metal system. The computation is carried out in two steps. First, the electric field is computed inside the defect by solving self-consistently Eq. (2). For this, GT connecting two points inside the metal must be numerically computed. Second, fields outside the defect are found using Eq. (2) again, with the previously computed electric field inside the defect. This involves GT connecting a point inside the metal half-space to a point in the vacuum half-space. In general, the computation of GT requires the numerical evaluation of a

difficult integral. However, only the asymptotic form of this GT is needed for the computation of T, R, and S. The asymptotic expressions for GT used are given in Appendix B.

III. SCATTERING BY A SINGLE DEFECT

Let us focus on inhomogeneities having a rectangular shape, with the following x dependency of the impedance:

$$\xi(x) = \begin{cases} \xi, & |x| > a/2 \\ \xi_i, & |x| \le a/2. \end{cases} \quad (3)$$

Such defects may be manufactured by inserting a metal wire with rectangular cross-section and impedance ξ_i into a thick conducting film with impedance ξ. We can assume the system to be homogeneous along the z direction when the wire depth is much larger than the skin depth, as explained in Sec. II C.

The normalized Fourier transform of the defect can be represented as $\eta_q = \Delta\xi \sin(qga/2)/\pi q$, where $\Delta\xi = \xi_i - \xi$. The SPP reflection coefficient, computed within the first-order Born approximation (FOBA) can be obtained by substituting $\eta_{-2q_{px}}$ into $r_{-q_{px}}$ (see Appendix A),

$$R_S = 4|r|^2 \sin^2\left(2\pi q_p \frac{a}{\lambda}\cos\theta\right), \quad (4)$$

where

$$r = \frac{\xi\Delta\xi}{2q_p^2}\frac{\cos 2\theta}{\cos^2\theta}. \quad (5)$$

Analogous to the reflection from the relief defect,[16] R_S presents the reflection coefficient r, associated with a single boundary of an impedance defect, multiplied by the interference factor. Notice that the dependence of r on the angle of incidence fully coincides with that of the p-polarization Fresnel coefficient at the boundary between two dielectrics (see Ref. 16). On the other hand, r for relief inhomogeneities does not depend on θ. As a result of this difference in the single boundary scattering coefficients, relief and impedance defects present different scattering properties. For example, while the reflectance from the relief defect decreases monotonically as θ decreases (at least for small a/λ),[16] the reflectance from an impedance barrier is essentially nonmonotone. A similar angular dependency was found for SPP scattering by a boundary to a uniform medium.[27]

Equation (4) yields two types of zeroes in the reflection coefficients, which appear as deep minima in the reflectance when going beyond the FOBA. The first zero of reflection arises from the vanishing of r. It appears at the angle of incidence $\theta_B = \pi/4$ and is independent of the size of the defect. This reflection minimum for SPPs is reminiscent of the zero reflectance at the Brewster angle appearing when a p-polarized wave impinges onto a dielectric interface. Its existence can be understood, *mutatis mutandis*, following the explanation for the appearance of the Brewster angle.

Consider a SPP impinging on an impedance defect. Since the impedance defect is located in the metal half-space, it can
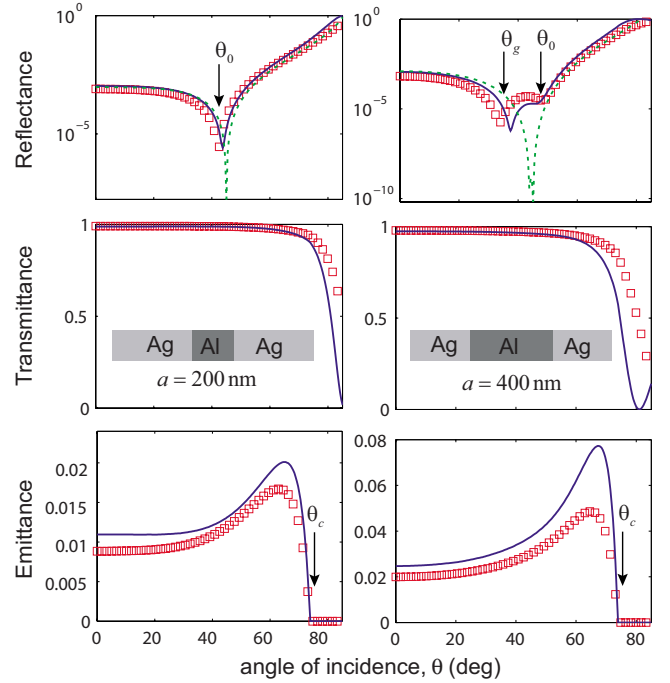
FIG. 2. (Color online) The SPP reflectance R, transmittance T, and emittance S as functions of the incident angle θ. A SPP impinges onto an aluminum stripe with a rectangular cross section placed in a thick silver slab. The defect widths are 200 nm in the left-hand panel and 400 nm in the right-hand panel. Results obtained within the Rayleigh approximation are rendered as solid curves (full calculation) and dashed lines (FOBA). The squares represent the results of GTA.

be represented by a polarization directed along the electric field of the SPP *inside the metal*. The field of the SPP inside the metal has a predominant longitudinal component parallel to the surface, with the z component being smaller by a factor of $1/\sqrt{\epsilon}$ (see Appendix C). Therefore, the polarization of an impedance barrier will point mainly in the direction of incidence. As shown in Appendix C, a dipole parallel to the surface emits SPPs primordially in the longitudinal direction, and not at all in the perpendicular direction. At $\theta_B = \pi/4$, the perpendicular direction coincides with the direction of reflection, so the reflection coefficient vanishes. For relief defects, however, the polarization mainly points along the direction normal to the surface as the incident SPP has a predominant z component above the metal. The radiation of SPPs by a point dipole in the vacuum half-space directed in the z direction is isotropically symmetric. This explains why in this case the reflection coefficient for an interface, r, does not depend on the angle of incidence (see Appendix C).

The second type of reflection minimum is given by the condition $2q_p(a/\lambda)\cos\theta_g = n$, where n is an integer. This reflectance minimum is due to interference: it occurs when the optical path of the plasmon inside the barrier is such that the amplitudes of reflected SPPs arising from the two ends of the barrier are in antiphase. Note that such optical path depends on both the angle of incidence and the barrier width.

Figure 2 represents the scattering coefficients for a SPP on an air-silver interface impinging onto an aluminum defect as a function of the angle of incidence. The left-hand and right-

hand panels show, respectively, the results for defects having widths of 200 and 400 nm. All dependencies have been calculated at $\lambda=600$ nm, taking ϵ from Ref. 28 ($\xi_{Ag}=-0.277i$, $\xi_{Al}=-0.146i$). The squares represent the results of GTA, while the solid curves were computed by solving integral equation (A4). In this calculation, the impedance obtained within the framework of SIBCs was adjusted to $\xi \to 1/\sqrt{1+\epsilon}$. With this minor change, the expression for q_p within the SIBCs coincides with the exact one.

Both cases considered in Fig. 2 exhibit Brewster-type reflectance minima at $\theta=\theta_B=45°$. FOBA (dashed curves in Fig. 2) predicts a vanishing R at $\theta=\theta_B$, while the exact solution gives a nonzero (but very deep) minimum.

The condition $a \gtrsim \lambda/2q_p$ is fulfilled by the 400-nm-wide defect, but it is not fulfilled by the 200-nm-wide defect. Correspondingly, the interference related dip is observed only in the former case. FOBA provides an estimation for the angular position of the interference reflection minimum; for the 400-nm-wide defect, FOBA predicts a dip at $\theta_g=43.9°$, while the minimum in the full calculation appears at $\theta_g=37.4°$.

The out-of-plane emittance in Fig. 2 shows the same pattern for the two defect widths considered. S initially increases with θ up to a maximum, whereafter it decreases and vanishes at the critical angle of incidence, θ_c. For angles larger than θ_c, the wave vector component k_y (which is conserved in the scattering) is larger than g, so there are no radiative modes the SPP can couple to. Notice that this critical angle appears for all frequencies at which the SPP exists, as the SPP has an in-plane wave vector larger than g. Clearly, the closer the SPP dispersion relation is to the light line, the closer θ_c gets to $\pi/2$. The out-of-plane emission can also be expressed in terms of the angle ϕ in Fig. 1, which characterizes the sector of possible directions of radiation within the continuum of propagating plane waves. Its dependency upon the angle of incidence and surface impedance, $\phi = 2\arccos(q_p \sin\theta)$, comes from simple geometrical considerations. At the critical angle of incidence, $\theta_c = \arcsin(1/\sqrt{1-\xi^2})$, ϕ vanishes and, consequently, $S=0$. In the region where $\theta \geq \theta_c$, only in-plane "elastic" SPP scattering takes place. For the parameters used in Fig. 2, $\theta_c = 73.91°$.

Figure 2 also shows that the difference between the results of GTA and Rayleigh expansion increases with the angle of incidence. At larger θ, the SPP is diverted to larger paths across the metal defect; therefore, the influence of the different treatment of boundary conditions by the two methods becomes more evident.

In order to stress the difference between impedance and surface relief scatterers, Fig. 3 presents GTA calculations for an aluminum protrusion of rectangular shape located on a silver surface. This inhomogeneity actually possesses the scattering properties inherent to both impedance and relief defects. In terms of the Rayleigh expansion approach, therefore, scattering cannot be described using either the potential for an impedance defect or that for a surface defect. Nevertheless, some scattering properties can be extended to this system from simpler systems with purely impedance and relief scatterers. No Brewster-type reflectance minima are exhibited by a relief perturbation, since the polarization induced in the defect points is mainly along the direction
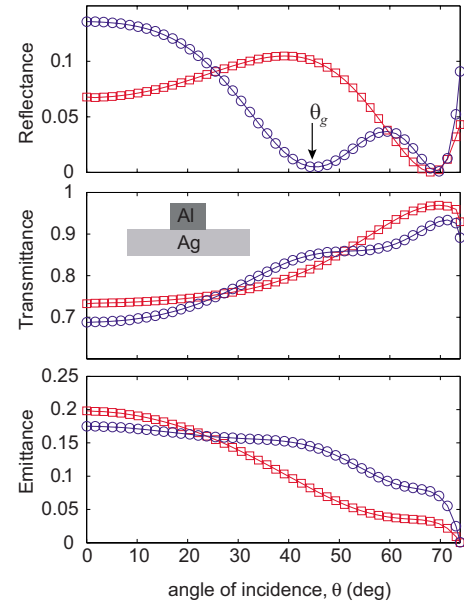
FIG. 3. (Color online) Scattering coefficients for an air-silver SPP impinging onto an Al protrusion of 40 nm height as a function of the angle of incidence. The squares (circles) are for protrusions with width of 200 (400) nm.

normal to the plane. However, the interference factor $\sin^2[2\pi q_p(a/\lambda)\cos\theta]$ also appears in this case in the reflection coefficient of the FOBA, so that a minimum in reflectance is expected at $\theta=\theta_g$. This minimum does, in fact, appear for the aluminum defect of 400 nm width, as shown in the numerical results in Fig. 3.

Also, note that the values of the reflectance and emittance for the scattering by a relief defect are much larger than those for the scattering by an impedance defect. This follows strictly from the form of the electric fields produced by dipoles in the metal or vacuum half-spaces. As we have explained, the effective polarization of the impedance defect points parallel to the metal surface, whereas that of the relief defect points perpendicularly to the surface. Therefore, according to Eqs. (C12) and (C13) of Appendix C, the modulus of the electric field corresponding to the dipole in the metal is $|\xi|$ times smaller than that corresponding to the dipole in the vacuum.

Finally, Fig. 4 illustrates the influence of the absorption on the reflection of SPPs by an impedance defect. Reflectivity is calculated using GTA. As Fig. 4 shows, absorption has a small effect on the reflection coefficient, whose amplitude is slightly reduced. The period of oscillations in the defect width is virtually unaltered.

IV. BRAGG MIRRORS

The reflectivity presented by an individual impedance barrier is very low, especially when close to the condition of normal incidence. In spite of that, a periodic array of impedance defects can create a band gap in the transmission. This is explainable by looking at the set of dominating maxima of the Fourier spectrum of the array located at $k=\pm k_n$, $k_n=nG$, where n is an integer, G is the modulus of the shorter
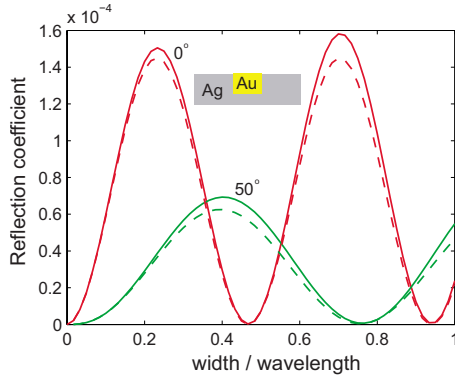
FIG. 4. (Color online) The SPP reflection coefficient R as a function of the defect width for two angles of incidence. The SPP impinges onto the gold rectangular inhomogeneity (with a depth of 40 nm) along the silver surface. The wavelength is 600 nm. The solid (dashed) curves are for the defect with (without) absorption.

Bragg vector $G=2\pi/d$, and d is the period of the array. Besides, according to FOBA (see Appendix A), the reflection coefficient is proportional to the Fourier transform of the array taken at $k=-2k_{px}$.[16] Therefore, for wavelengths $\lambda_n=2dq_p\cos\theta/n$, the incoming and reflected SPPs are strongly coupled. In other words, this implies that the phase difference of waves emitted by two neighboring barriers is divisible by π, so that SPP wave fields launched by all barriers interfere constructively. Thus, close to wavelengths λ_n, the reflection coefficient increases dramatically and, in turn, the transmission and out-of-plane scattering coefficients decrease to satisfy energy conservation.

An example of the wavelength spectra computation at different angles is shown in Fig. 5. A SPP impinges onto 20 aluminum defects periodically located in the background silver. The evolution of the reflectance peak corresponding to the fundamental band gap in the vicinity of λ_1 is illustrated. As seen in the figure, the amplitude of the maximum is a nonmonotonic function of θ. Such behavior can be analyzed by computing the reflectance within FOBA. Substituting λ_n into the analytic expression for the reflectivity, we find that the angular dependency of the maximum of R located near the nth band gap for N scatterers is

$$R_{\max,n}=N^2\frac{|\xi\Delta\xi|^2}{q_p^4}\frac{\cos^2 2\theta}{\cos^4\theta}\sin^2(\pi na/d). \quad (6)$$

Here, the quantities ξ, $\Delta\xi$, and q_p must be taken at $\lambda=\lambda_n(\theta)$. According to the general property of scattering by an impedance defects, previously discussed, the reflection coefficient vanishes when $\theta=\pi/4$. This is clearly seen in Fig. 5, wherein Eq. (6) is plotted by the dashed curve as a function of the "resonant" wavelength λ_1. The normalized coefficient is chosen so that Eq. (6) coincides with the numerically computed maxima at $\theta=20°$ and $\theta=40°$.

It is interesting to note that the widths of reflection peaks depend on the angle of incidence. Within FOBA, the half-width $\Delta\lambda_{hw}$ of reflection maxima for an array of impedance defects can be computed from the condition $R(\lambda_n)/R(\lambda_n+\Delta\lambda_{hw})=2$. Neglecting the variation of the impedance in
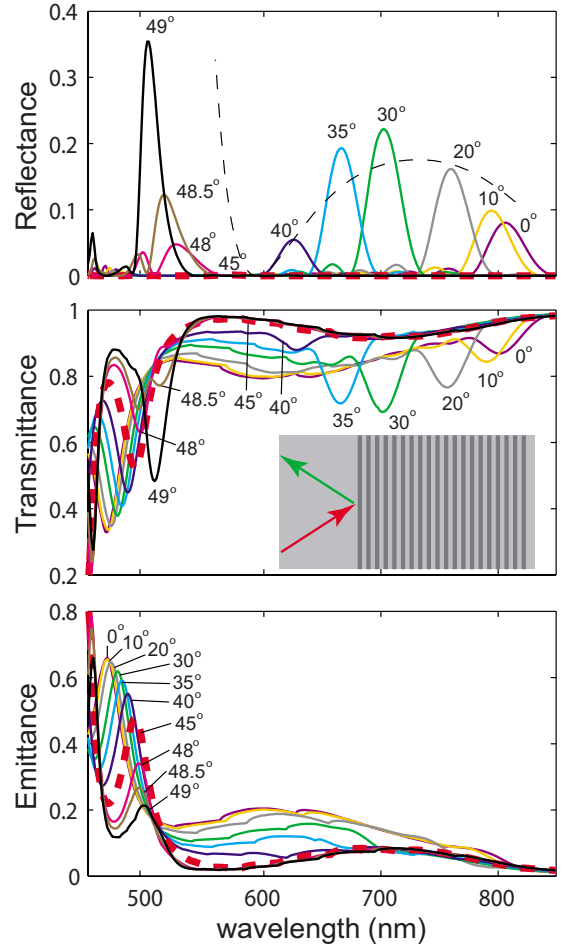
FIG. 5. (Color online) The wavelength spectra of the scattering coefficients computed by using Rayleigh expansion. A SPP impinges onto 20 periodically located aluminum rectangular defects inserted into silver. The period of the array is $d=400$ nm, and the width of the single defect is $a=200$ nm. The labels over the curves correspond to the values of the incidence angle θ in degrees.

such a narrow wavelength range, we obtain $\Delta\lambda_{hw}\sim\cos\theta$. This coincides with the corresponding dependency for relief Bragg scatterers. In terms of the angle ψ between $\mathbf{k}_{pt}$ and $\mathbf{k}_{pt}^R$, the half-width of the reflection maxima scales as $\Delta\lambda_{hw}\sim\sin(\psi/2)$.[16] It is worth stressing that $\Delta\lambda_{hw}$ and the width of the SPP band gap in a periodic lattice of defects, $\Delta\lambda_{bg}$, can have different angular dependencies. For example, the band gap width of the impedance grating depends on θ as $\Delta\lambda_{bg}\sim\cos 2\theta$ ($\sim\cos\psi$),[18,19] so that it vanishes at $\psi=\pi/2$ ($\theta=\pi/4$). Thus, the uncoupling between SPPs with mutually perpendicular wave vectors affects a finite impedance Bragg mirror differently from periodic impedance gratings. Namely, the uncoupling causes the vanishing of SPP reflection for Bragg scatterers and closes the band gap for gratings. Conversely, for structures with corrugated relief, the dependencies on the angle of incidence of $\Delta\lambda_{hw}$ and $\Delta\lambda_{bg}$ coincide.

V. CONCLUSIONS

We have presented a theoretical investigation of oblique SPP scattering by 1D impedance defects and have contrasted

the results to those of relief defects. Calculations have been performed within (i) Green's dyadic method (which is virtually exact if small enough values of the mesh are used) and (ii) the Rayleigh expansion, in which surface impedance boundary conditions have been imposed. The quality of the agreement obtained with both methods validates the use of the approximate scheme. Additionally, we have given approximate analytical expressions for the different scattering coefficients obtained within the first-order Born approximation.

The presented results display a net distinction between SPP scattering by impedance defects and SPP scattering by shallow indentations or protrusions. While scattering by impedance defects presents a Brewster-type deep reflectance minimum, for angles of incidence $\theta \approx \pi/4$, scattering by either protrusions or indentations do not show this effect. Such distinction has been shown to arise from the different polarizations induced by the incoming SPP at the position of the defect. The polarization induced in an impedance barrier points in the direction of incidence mainly, while the polarization induced in a relief defect predominantly points perpendicular to the surface. Both relief and impedance defects with rectangular shape exhibit low reflectance for certain angles of incidence for which the SPP waves reflected from the two ends of the barrier interfere destructively.

Arrays of impedance defects have also been considered. It has been shown that the reflectance of these arrays can be large for angles different from the SPP Brewster-type angle $\theta_B \approx \pi/4$.

ACKNOWLEDGMENTS

APPENDIX A: RAYLEIGH EXPANSION

In this appendix, we derive the integral equations that describe the scattering of SPP by impedance defects. The derivations can be followed by the same lines of arguments already presented in the case of relief defects.[16]

SIBCs at the interface $z=0$ read as

$$\mathbf{E}_t(\mathbf{r}) + \xi(x)[\mathbf{e}_z \times \mathbf{H}] = 0, \qquad (A1)$$

where the subscript t stands for the tangential-to-the-surface components of the vector. Using Maxwell's equation, $\mathbf{H} = (ig)^{-1}[\nabla \times \mathbf{E}]$, Eq. (A1) becomes

$$\mathbf{E}_{kt} + \int \frac{dk'}{g} \xi_{k-k'}[\mathbf{e}_z \times (\mathbf{K}' \times \mathbf{E}_{k'})]$$

$$= -\delta(k - k_{px})\mathbf{e}_{pt} - \frac{\xi_{k-k_{px}}}{g}[\mathbf{e}_z \times (\mathbf{k}_p \times \mathbf{e}_p)]. \quad (A2)$$

Here, ξ_k is the Fourier transform of the surface impedance $\xi(x)$, which is conveniently written as $\xi_k = \delta(k)\xi + \tilde{\xi}_k$; $\delta(k)$ is

the delta function. Normalizing the electric fields using Green's functions for p polarization, $G_q^- = 1/(\xi + q_z)$ (where the normalized x and z components of the wave vectors are $q = k/g$ and $q_z = k_z/g$, respectively) and for s polarization, $G_q^+ = 1/(1 + \xi q_z)$, we can write the field as

$$\mathbf{E}_k = g^{-1} \sum_\sigma G_q^\sigma r_q^\sigma \mathbf{e}_q^\sigma. \qquad (A3)$$

The binary variable $\sigma = + \ (-)$ indicates $s \ (p)$ polarization so that if we designate $\mathbf{q}_t = (q, q_p \sin\theta, 0)$, the polarization basis vectors for each plane wave are $\mathbf{e}_q^+ = \mathbf{e}_z \times \mathbf{q}_t/q_t$ and $\mathbf{e}_q^- = \mathbf{e}_q^+ \times \mathbf{K}/g$. Projecting Eq. (A2) onto two mutually perpendicular directions along the vectors $\mathbf{q}_t$ and $\mathbf{e}_q^+$, analogous to what was done in Ref. 16, we arrive at a pair of coupled integral equations for the normalized field harmonics,

$$r_q^\sigma + \sum_{\sigma'} \int dq' U_{qq'}^{\sigma\sigma'} G_{q'}^{\sigma'} r_{q'}^{\sigma'} = -U_{qq_{px}}^{\sigma-}. \qquad (A4)$$

In these formulas, $q_{px} = q_p \cos\theta$. The potential describing the SPP-defect interaction has the following compact form:

$$U_{qq'}^{\sigma\sigma'} = \sigma'^{(1+\sigma)/2} \eta_{q-q'} S_{qq'}^{\sigma\cdot\sigma'} q_z'^{(1+\sigma')/2}. \qquad (A5)$$

The coefficients $S_{qq'}^+ = \mathbf{q}_t \cdot \mathbf{q}_t'/q_t q_t'$ and $S_{qq'}^- = \mathbf{e}_z \cdot (\mathbf{q}_t \times \mathbf{q}_t')/q_t q_t'$ are the cosine and sine of the angle between the vectors $\mathbf{q}_t$ and $\mathbf{q}_t'$, respectively. The normalized Fourier image of the inhomogeneity is $\eta_q = g\tilde{\xi}_k$.

The spatial dependency in the asymptotic region $x \to \infty$ is given by the propagating transmitted SPP,

$$\mathbf{E}(\mathbf{r}) = \mathbf{e}_p(1 + \tau)\exp(i\mathbf{k}_p \cdot \mathbf{r}), \qquad (A6)$$

while when $x \to -\infty$, the spatial field distribution results from the interference between the incoming and the reflected SPPs, the latter having a wave vector $\mathbf{k}_p^R = g(-q_{px}, q_p \sin\theta, \xi)$,

$$\mathbf{E}(\mathbf{r}) = \mathbf{e}_p \exp(i\mathbf{k}_p \cdot \mathbf{r}) + \rho \mathbf{e}_{-q_{px}}^- \exp(i\mathbf{k}_p^R \cdot \mathbf{r}). \qquad (A7)$$

The amplitude of the reflected SPP, ρ, and the term contributing to the amplitude of the transmitted SPP, τ, can be extracted from Eqs. (1) and (A3), prolonging the integrands to the complex plane and taking into account the presence of the poles. Only the poles of Green's function for p polarization, $\xi + q_z = 0$, contribute to the result of the integration since physically they yield the SPP dispersion relation of the interface without defects. Integrating, we obtain that ρ and τ are related to r_q^σ as $\rho = (2\pi i \xi/q_{px})r_{-q_{px}}^-$ and $\tau = (2\pi i \xi/q_{px})r_{q_{px}}^-$. From here, both reflection, $R = |\rho|^2$, and transmission, $T = |1 + \tau|^2$, coefficients are derived. The out-of-plane scattering coefficient is obtained from integration over the continuum of homogeneous waves of the electric field amplitude squared, with both s- and p-polarized fields contributing to the final result,

$$S = \frac{4\pi|\xi|}{q_{px}} \sum_\sigma \int_{\text{Im}(q_z)=0} dq q_z |G_q^\sigma r_q^\sigma|^2. \qquad (A8)$$

Hence, Eq. (A8) allows for polarization conversion at SPP scattering. Changing $dq \to q_t d\varphi$, where φ is the polar angle

in the x-y plane taken from the vector $\mathbf{k}_{pt}$, the coefficient S can be written as an integral of the scattering cross section $D(\varphi)$,

$$S = \int_0^{\phi} d\varphi D(\varphi), \quad \text{where} \quad \phi = 2\arccos(q_p \sin\theta). \tag{A9}$$

Integral equation (A4) can be solved numerically, discretizing the integrands and restricting the region of the integration. The discretization step and the restriction of the upper and lower limits of the integrals are determined by the convergency of the result and the numerical precision to which the law of conservation of energy: $S+R+T=1$ is fulfilled. Along with the numeric solution, it is useful to write r_q^{σ} in the form of a perturbational series in the parameter η_q. FOBA is attained from Eq. (A4) once the integral term has been suppressed,[15,16]

$$r_q^{\sigma(B)} = -U_{qq_{px}}^{\sigma-} = \sigma\eta_{q-q_{px}}S_{qq_{px}}^{-\sigma}. \tag{A10}$$

Thus, the qth field Fourier amplitude is both proportional to the "coupling" harmonic of the inhomogeneity, $\eta_{q-q_{px}}$, and to the angular coefficient. The latter is related to the scalar product of tangential components of the electric field of the SPP and the scattered wave.

APPENDIX B: GREEN'S TENSOR APPROACH

The two-dimensional (2D) Green's tensor for the case in which $k_y=k_{py}$ is cyclic couples a point (x',z') inside the metal to a point (x,z) in the vacuum half-space and can be represented as a Sommerfeld integral:[29]

$$\hat{\mathbf{G}}(\Delta x, z, z') = \frac{i}{4\pi}\int_{-\infty}^{\infty} dk\, e^{i(k\Delta x+k_z z-k_z^m z')}\hat{\mathbf{\Phi}}(k), \tag{B1}$$

where $\Delta x = x-x'$, $k_z^m = \sqrt{\epsilon g^2-k^2-k_{py}^2}$, and

$$\hat{\mathbf{\Phi}}(k) = (k_z^m)^{-1}[t_p(k)\hat{\mathbf{\Gamma}}_p(k) + t_s(k)\hat{\mathbf{\Gamma}}_s(k)]. \tag{B2}$$

$t_p(k)$ and $t_s(k)$ are the Fresnel transmission coefficients of plane waves at a metal-air interface for the p and s polarizations, respectively: $t_p(k) = 2k_z\sqrt{\epsilon}(k_z^m+\epsilon k_z)^{-1}$ and $t_s(k) = 2k_z^m(k_z^m+k_z)^{-1}$.

$$\hat{\mathbf{\Gamma}}_p(k) = Y_p\begin{pmatrix} k^2 & kk_{py} & -kk_t^2/k_z^m \\ kk_{py} & k_{py}^2 & -k_t^2 k_{py}/k_z^m \\ -kk_t^2/k_z & -k_t^2 k_{py}/k_z & k_t^4/k_z^m k_z \end{pmatrix}, \tag{B3}$$

$$\hat{\mathbf{\Gamma}}_s(k) = Y_s\begin{pmatrix} k_{py}^2 & -kk_{py} & 0 \\ -kk_{py} & k^2 & 0 \\ 0 & 0 & 0 \end{pmatrix}, \tag{B4}$$

where $Y_p = k_z k_z^m/g^2\sqrt{\epsilon}k_t^2$ and $Y_s = 1/k_t^2$.

The integral in Eq. (B1) is well defined if the analytical structure of the integrand is properly taken into account. Mathematically, this is required because the integrand contains square roots such as $k_z = \sqrt{g^2-k^2-k_{py}^2}$. These terms pro-
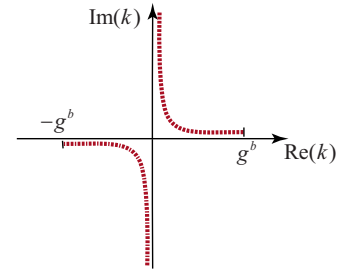
FIG. 6. (Color online) Schematic of the branch cuts of k_z in the complex k plane when the radiation regions have infinitesimal absorption; $g^b = \sqrt{g^2-k_{py}^2}$.

duce branch cuts on the axis $\text{Re}(k)$, so direct integration (B1) along this axis is in principle meaningless. The correct prescription for evaluating Eq. (B1) can be obtained in three steps: (a) Consider that the media in the radiation regions have infinitesimal absorption. This translates into a small imaginary part under the square roots (e.g., $k_z = \sqrt{g^2-k^2-k_{py}^2+i\eta}$). (b) Perform the integral for a finite η. (c) Take the limit of the result as η tends to zero. The addition of η under the square roots (in step a), modifies the analytical structure of the integrand of Eq. (B1): branch cuts are displaced away from the real $\text{Re}(k)$ in the way represented in Fig. 6 (we have taken the branch cut of $\sqrt{z}$ in the real z axis). It is now possible to define the integral along this axis. Actually, the limit $\eta\to 0$ can be taken in the integrand provided the cited branch cuts are not crossed if, as is customary,[30] the integration path is deformed into the complex k plane.

An additional singularity of the integrand defining $\hat{\mathbf{G}}$ is the pole in $t_p(k)$ at $k=k_{px}$, defined by the condition $k_z^m = -\epsilon k_z$. This singularity corresponds to the SPP of the interface and can be extracted applying the residue theorem to Eq. (B1). The resulting GT has the form

$$\hat{\mathbf{G}}_{\text{spp}}(\Delta x, z, z') = G_p e^{i[k_{px}\Delta x-k_{pz}z-k_{pz}^m z']}\hat{\mathbf{\Gamma}}_p(k_{px}), \tag{B5}$$

where

$$G_p = -\frac{\sqrt{\epsilon}}{\epsilon^2-1}\frac{k_{pz}^m}{k_{px}}, \tag{B6}$$

where $k_{pz}^m \equiv \sqrt{\epsilon g^2-k_{px}^2-k_{py}^2}$. This contribution dominates in the limit $x\gg\lambda, z\sim 0, z'\sim 0$, so $\hat{\mathbf{G}}(x\gg\lambda, z\sim 0, z'\sim 0) \approx \hat{\mathbf{G}}_{\text{spp}}(\Delta x\sim 0, z'\sim 0)$.

The other asymptotic limit is the far field away from the plane: $x\to\pm\infty, z\to-\infty$, or in polar coordinates $x=R\cos\alpha, z=-R\sin\alpha$, and $R\to\infty$. Applying the method of the steepest descent to the Sommerfeld integral, we recover the limit of geometrical optics, whereby Green's tensor (B1) is reduced to a function of the minimal optical path wavevector $\boldsymbol{\kappa}$,

$$\hat{\mathbf{G}}_{\text{rad}}(\mathbf{r}, \mathbf{r}') = e^{-i(\kappa_x x'+\kappa_z^m z')}\frac{e^{i(\gamma R+\pi/4)}}{\sqrt{8\pi\gamma R}}\hat{\mathbf{G}}^{\infty}(\kappa_x), \tag{B7}$$

where $\boldsymbol{\kappa} = (\kappa_x, k_{py}, \kappa_z) = (\boldsymbol{\kappa}_t, \kappa_z)$, with $\kappa_x = \gamma\cos\alpha$, $\kappa_z = \gamma\sin\alpha$, and $\gamma = \sqrt{g^2-k_{py}^2}$ in the air half-space $z<0$; while $\kappa_z^m = \sqrt{\epsilon g^2-k_{py}^2-\gamma^2\cos^2\alpha}$ in the metal half-space $z>0$.

$\hat{\mathbf{G}}^{\infty}(\kappa_x)$ has contributions from both p and s polarizations as

$$\hat{\mathbf{G}}^{\infty}(\kappa_x) = t_p(\kappa_x)\hat{\mathbf{\Gamma}}_{\mathbf{p}}(\kappa_x) + t_s(\kappa_x)\hat{\mathbf{\Gamma}}_s(\kappa_x). \quad \text{(B8)}$$

APPENDIX C: COUPLING OF SURFACE PLASMON POLARITONS TO A POINT DIPOLE

We will now deduce the SPP excitation produced by a dipole placed in either the vacuum half-space or the metal half-space. In Appendix B, we have highlighted that the singularity of $\hat{\mathbf{G}}$ in Eq. (B5), related to the coupling with SPPs, can be extracted from the 2D Sommerfeld integral (B1) as a residue. Equation (B5) represents the excitation of SPPs produced by a polarized strip source (having infinite extension in the y direction).

Similarly, the coupling of a point dipole to SPPs is given by the relevant pole in the Green's tensor. This is extracted from a three-dimensional (3D) Sommerfeld integral, wherein integration must be carried out over both k_x and k_y, as no constraint is imposed on k_y. The 3D Sommerfeld integrals for a dipole in either half-spaces can be found in the literature; see, for instance, Sec. (10.4) of Ref 31. The case of a dipole in the vacuum half-space has been considered in detail in Refs. 17 and 29.

Let us sketch here the derivation for the expression of the coupling between a dipole placed close to the interface and a surface plasmon polariton. The electric field produced by a point dipole source $\mathbf{p}$ placed at the origin is directly related to Green's tensor as

$$\mathbf{E}(\mathbf{r}) = g^2 \hat{\mathbf{G}}(\mathbf{r},0) \cdot \mathbf{p}. \quad \text{(C1)}$$

Correspondingly, the electric field of surface plasmons radiated by the dipole can be obtained from

$$\mathbf{E}_{\text{spp}}(\mathbf{r}) = g^2 \hat{\mathbf{G}}_{\text{spp}}(\mathbf{r},0) \cdot \mathbf{p}, \quad \text{(C2)}$$

where $\hat{\mathbf{G}}_{\text{spp}}$ is the contribution of the surface plasmon pole to $\hat{\mathbf{G}}$.

In general, Green's tensor is constructed by an eigenmode expansion on both p-polarized and s-polarized plane waves, but the SPP pole appears only in relation to the p-polarization part. The electric field vector of a p-polarized plane wave having a wave vector $\mathbf{k}$ and satisfying the radiation condition at $\pm\infty$ is given by the unitary vector $\mathbf{k}_{\pm}^v$ (in vacuum) or $\mathbf{k}_{\pm}^m$ (inside the metal). In particular, the coupling of the field of the dipole with SPPs is obtained through the eigenmodes $\mathbf{k}_{\pm}^v$ and $\mathbf{k}_{\pm}^m$ fulfilling the dispersion relation of a SPP. The expressions for $\mathbf{k}=\mathbf{k}_p$ of these unitary vectors are

$$\mathbf{k}_{\pm}^v = \frac{k_{pz}}{gk_{pt}}\begin{pmatrix} k_{px} \\ k_{py} \\ \mp k_{pt}^2/k_{pz} \end{pmatrix}, \quad \text{(C3)}$$

$$\mathbf{k}_{\pm}^m = \frac{k_{pz}^m}{g\sqrt{\epsilon}k_{pt}}\begin{pmatrix} k_{px} \\ k_{py} \\ \mp k_{pt}^2/k_{pz}^m \end{pmatrix}. \quad \text{(C4)}$$

In order to calculate $\hat{\mathbf{G}}_{\text{spp}}(\mathbf{r},\mathbf{r}')$, special care must be paid to whether the source at $\mathbf{r}'$ is placed in the vacuum or in the metal and, similarly, whether we calculate the fields at a point $\mathbf{r}$ in the vacuum or in the metal. We denote by $\hat{\mathbf{G}}_{\alpha,\beta}(\mathbf{r}) = \hat{\mathbf{G}}_{\text{spp}}(\mathbf{r},\mathbf{r}' \to 0)$, where $\alpha=v,m$ if we calculate the fields in vacuum or the metal, respectively (and $\beta=v,m$ depending on whether the dipole is placed just outside or just inside the metal, respectively).

Then, following Eqs. (20)–(24) of Ref. 29 we arrive at

$$\hat{\mathbf{G}}_{\alpha,\beta}(\mathbf{r}) = e^{i(k_{p}r_{\parallel}-\pi/4)}\sqrt{\frac{k_{pt}}{2\pi r_{\parallel}}}\frac{\epsilon}{\epsilon^2-1}\frac{k_{pz}}{k_{pt}}\hat{\mathbf{g}}_{\alpha,\beta}, \quad \text{(C5)}$$

$$\hat{\mathbf{g}}_{v,v} = -\epsilon e^{-ik_{pz}z}\mathbf{k}_-^v\mathbf{k}_+^v, \quad \text{(C6)}$$

$$\hat{\mathbf{g}}_{v,m} = \sqrt{\epsilon}e^{ik_{pz}^m z}\mathbf{k}_+^m\mathbf{k}_+^v, \quad \text{(C7)}$$

$$\hat{\mathbf{g}}_{m,v} = \sqrt{\epsilon}e^{-ik_{pz}z}\mathbf{k}_-^v\mathbf{k}_-^m, \quad \text{(C8)}$$

$$\hat{\mathbf{g}}_{m,m} = -e^{ik_{pz}^m z}\mathbf{k}_+^m\mathbf{k}_-^m. \quad \text{(C9)}$$

These results can be expressed in a more compact form if we define an (arbitrarily normalized) surface plasmon polariton field in both vacuum ($z<0$) and metal ($z>0$) half-spaces as

$$\mathbf{e}_{\text{spp}}(\mathbf{r}) = \begin{pmatrix} \xi\cos\theta \\ \xi\sin\theta \\ -1 \end{pmatrix} e^{i(k_{px}x+k_{py}y-k_{pz}z)}, \quad z<0, \quad \text{(C10)}$$

$$\mathbf{e}_{\text{spp}}(\mathbf{r}) = \begin{pmatrix} \xi\cos\theta \\ \xi\sin\theta \\ -\xi^2 \end{pmatrix} e^{i(k_{px}x+k_{py}y+k_{pz}^m z)}, \quad z>0. \quad \text{(C11)}$$

The final expressions are the following:
(a) for a dipole placed in the vacuum side of the metal-vacuum interface,

$$\mathbf{E}_{\text{spp}}(\mathbf{r}) = \widetilde{Z}g^2\sqrt{\frac{k_{pt}}{2\pi i r_{\parallel}}}(\xi\mathbf{p}\cdot\mathbf{e}_{\parallel}+\mathbf{p}\cdot\mathbf{e}_z)\mathbf{e}_{\text{spp}}(\mathbf{r}), \quad \text{(C12)}$$

(b) for a dipole placed in the metal side of the metal-vacuum interface,

$$\mathbf{E}_{\text{spp}}(\mathbf{r}) = \widetilde{Z}g^2\sqrt{\frac{k_{pt}}{2\pi i r_{\parallel}}}(\xi\mathbf{p}\cdot\mathbf{e}_{\parallel}+\xi^2\mathbf{p}\cdot\mathbf{e}_z)\mathbf{e}_{\text{spp}}(\mathbf{r}),$$

$$\text{(C13)}$$

where $\widetilde{Z}=\frac{\xi}{(1+\xi^2)(\xi^4-1)}$. Therefore, a dipole oriented along the interface emits plasmons preferentially in the longitudinal direction and does not radiate SPPs in the perpendicular direction. By contrast, a dipole placed at the surface but oriented along its normal direction radiates plasmons isotropically in the plane.

*alexeynik@rambler.ru

†lmm@unizar.es

[1] J. Vuckovic, M. Loncar, and A. Scherer, IEEE J. Quantum Electron. **36**, 1131 (2000).

[2] S. I. Bozhevolnyi, V. S. Volkov, E. Devaux, J.-Y. Laluet, and T. W. Ebbesen, Nature (London) **440**, 508 (2006).

[3] J.-C. Weeber, J. R. Krenn, A. Dereux, B. Lamprecht, Y. Lacroute, and J. P. Goudonnet, Phys. Rev. B **64**, 045411 (2001).

[4] W. L. Barnes, A. Dereux, and T. W. Ebbesen, Nature (London) **424**, 824 (2003).

[5] S. A. Maier, Curr. Nanosci. **1**, 17 (2005).

[6] A. V. Shchegrov, I. V. Novikov, and A. A. Maradudin, Phys. Rev. Lett. **78**, 4269 (1997).

[7] J. A. Sánchez-Gil, Appl. Phys. Lett. **73**, 3509 (1998).

[8] J. A. Sánchez-Gil and A. A. Maradudin, Phys. Rev. B **60**, 8359 (1999).

[9] F. López-Tejeira, F. J. García-Vidal, and L. Martín-Moreno, Phys. Rev. B **72**, 161405(R) (2005).

[10] M. U. González, J.-C. Weeber, A.-L. Baudrion, A. Dereux, A. L. Stepanov, J. R. Krenn, E. Devaux, and T. W. Ebbesen, Phys. Rev. B **73**, 155416 (2006).

[11] A. Drezet, A. L. Stepanov, A. Hohenau, B. Steinberger, N. Galler, H. Ditlbacher, A. Leitner, F. R. Aussenegg, J. R. Krenn, M. U. Gonzalez, and J.-C. Weeber, Europhys. Lett. **74**, 693 (2006).

[12] J. Gómez Rivas, M. Kuttge, H. Kurz, P. Haring Bolivar, and J. A. Sánchez-Gil, Appl. Phys. Lett. **88**, 082106 (2006).

[13] A. B. Evlyukhin, S. I. Bozhevolnyi, A. L. Stepanov, and J. R. Krenn, Appl. Phys. B: Lasers Opt. **84**, 29 (2006).

[14] J. Gaspar-Armenta, R. García-Llamas, and J. Durán-Favela, Phys. Rev. B **73**, 155412 (2006).

[15] A. Yu. Nikitin, F. López-Tejeira, and L. Martín-Moreno, Phys. Rev. B **75**, 035129 (2007).

[16] A. Y. Nikitin and L. Martín-Moreno, Phys. Rev. B **75**, 081405(R) (2007).

[17] A. B. Evlyukhin, G. Brucoli, L. Martín-Moreno, S. I. Bozhevolnyi, and F. J. García-Vidal Phys. Rev. B **76**, 075426 (2007).

[18] A. V. Kats and A. Y. Nikitin, Proc. SPIE **5221**, 218 (2003).

[19] A. V. Kats, M. L. Nesterov, and A. Y. Nikitin, Phys. Rev. B **76**, 045413 (2007).

[20] M. U. González, A. L. Stepanov, J.-C. Weeber, A. Hohenau, A. Dereux, R. Quidant, and J. R. Krenn, Opt. Lett. **32**, 2704 (2007).

[21] H. W. Hohmann, Geophysics **40**, 309 (1975).

[22] G. Protásio, D. A. Rogers, and A. J. Giarola, Radio Sci. **17**, 503 (1982).

[23] O. Keller, Phys. Rev. B **34**, 3883 (1986).

[24] L. W. Li, J. A. Bennet, and P. L. Dyson, Int. J. Electron. **70**, 803 (1991).

[25] L. Novotny, J. Opt. Soc. Am. A **14**, 105 (1997).

[26] O. J. F. Martin and N. B. Piller, Phys. Rev. E **58**, 3909 (1998).

[27] R. Gordon, Phys. Rev. B **74**, 153417(B) (2006).

[28] *Handbook of Optical Constants of Solids*, edited by E. D. Palik (Academic Press, New York, 1985).

[29] T. Sondergaard and S. I. Bozhevolnyi, Phys. Rev. B **69**, 045422 (2004).

[30] M. Paulus, P. Gay-Balmaz, and O. J. F. Martin, Phys. Rev. E **62**, 5797 (2000).

[31] L. Novotny and B. Hecht, *Principles of Nano-Optics* (Cambridge University Press, Cambridge, 2006).